Synthesis and materialization of a reaction-diffusion French flag pattern

Anton Zadorin, Yannick Rondelez, Guillaume Gines, Vadim Dilhas, Georg Urtel, Adrian Zambrano, Jean-Christophe Galas, André Estévez-Torres

Synthesis and materialization of a reaction-diffusion French flag pattern

Anton S. Zadorin[1,2], Yannick Rondelez[3,4], Guillaume Gines[3], Vadim Dilhas[1,2], Georg Urtel[5], Adrian Zambrano[1,2], Jean-Christophe Galas[1,2,*], André Estevez-Torres[1,2,*]

[1]Université Pierre et Marie Curie, Laboratoire Jean Perrin, 4 place Jussieu, 75005 Paris, France. [2]CNRS, UMR 8237, 75005, Paris, France. [3]LIMMS/CNRS-IIS, University of Tokyo, Komaba 4-6-2 Meguro-ku, Tokyo, Japan. [4]Ecole supérieure de physique et chimie industrielle, Laboratoire Gulliver, 10 rue Vauquelin, 75005, Paris, France. [5] Ludwig-Maximilians-Universität München, Fakultät für Physik, Amalienstraße 54, 80799 Munich, Germany

*To whom correspondence should be addressed;

E-mail: jean-christophe.galas@upmc.fr, andre.estevez-torres@upmc.fr.

During embryo development, patterns of protein concentration appear in response to morphogen gradients. These patterns provide spatial and chemical information that directs the fate of the underlying cells. Here, we emulate this process within non-living matter and demonstrate the autonomous structuration of a synthetic material. Firstly, we use DNA-based reaction networks to synthesize a French flag, an archetypal pattern composed of three chemically-distinct zones with sharp borders whose synthetic analogue has remained elusive. A bistable network within a shallow concentration gradient creates an immobile, sharp and long-lasting concentration front through a reaction-diffusion mechanism. The combination of two bistable circuits generates a French flag pattern whose 'phenotype' can be reprogrammed by network mutation. Secondly, these concentration patterns control the macroscopic organization of DNA-decorated particles, inducing a French flag pattern of colloidal aggregation. This experimental framework could be used to test reaction-diffusion models and fabricate soft materials following an autonomous developmental program.

From a chemist's perspective, biological matter has the astonishing capability of self-constructing into shapes that are predetermined, robust to varying environmental conditions and remarkably pre-

cise in size and chemical composition at different scales. Living embryos, for instance, develop from a simple form into a complex one through a reproducible process called embryogenesis. The embryo is first structured chemically through pattern formation, a process during which out-of-equilibrium molecular programs generate highly ordered concentration patterns of μm to mm size.[1] Subsequent developmental steps involve morphogenesis, where the embryo changes its shape, cell differentiation, in which cells become structurally and functionally different, and finally growth, resulting in an increase of the mass of the embryo.[1] The emulation of such processes in non-living chemical systems adresses two important goals. First, in a reductionist perspective, it allows testing theoretical models describing the emergence of out-of-equilibrium material order in simplified experimental conditions.[2] Second, from a synthetic standpoint, it enables the conception of a new way of making soft materials[3,4] that one may call 'artificial development': materials that build themselves following a pre-encoded molecular program.

The first developmental step, pattern formation, is currently interpreted in the light of two archetypal scenarios: Turing's instability[5] and Wolpert's processing of positional information.[6] The Turing scenario implies an initially homogeneous reaction-diffusion (RD) system that spontaneously breaks the symmetry, generating repetitive structures of wavelength $\sqrt{D\tau}$, where D is a diffusion coefficient and τ a characteristic reaction time. In Wolpert's scenario, instead, the symmetry is already broken by a pre-existing morphogen gradient that is subsequently interpreted in a threshold-dependent manner, producing several chemically-distinct regions with sharp borders. Lewis Wolpert named this the French flag problem to illustrate the issue of creating three distinct regions of space —the head, the thorax and the abdomen— from an amorphous mass and a shallow concentration gradient (Fig. 1a). Historically, Turing's and Wolpert's scenarios have been considered mutually exclusive,[7] the first needing diffusion in contrast with the second. However, recent hypothesis suggest that both scenarios could be combined during development[7] and that diffusion could make the processing of positional information more robust.[8,9] The experimental proof of the Turing mechanism in vivo has met constant criticism,[7] although recent work has provided new evidence.[10,11] In contrast, Wolpert's scenario is accepted in living embryos, possibly because it is more loosely defined. Well-known examples are provided by the gap gene system in *Drosophila*[12] and by the sonic hedgehog-induced patterning of

the vertebrate neural tube.[13] Concerning non-living systems, Turing patterns were first demonstrated experimentally in 1990[14] whereas synthetic systems capable of interpreting a morphogen pre-pattern have remained elusive.

Here, we draw inspiration from pattern formation during early *Drosophila* development to address a synthetic challenge: can one build a French flag pattern outside of a living organism? In a learning-by-doing approach[15–20] to this question our synthetic route combines reaction-diffusion with positional information, Turing and Wolpert ideas, suggesting that these two mechanisms are not antinomic. Furthermore, by considering pattern formation in the context of development as a blueprint for cell differentiation we ask a second question: may a self-organized chemical pattern influence the final structure of an initially homogeneous material? In doing this, we demonstrate that a soft material can be autonomously structured through an artificial developmental program.

Results

The conversion of a shallow morphogen gradient into a concentration boundary that is both sharp and immobile requires a reaction network that interprets the gradient in a non-linear fashion. Diverse evidence[8,21–23] suggests that bistability is an essential property of such networks and that coupling bistability with diffusion provides immobile and robust fronts.[8,9,23] Our design for building a French flag pattern thus consists of two bistable networks that generate two RD fronts of concentration pinned in a gradient of a bifurcation parameter.

DNA oligonucleotides are particularly well-suited to construct pattern-forming reaction networks.[17,18,24,25] The reactivity of the hybridization reaction obeys simple rules and a wide array of methods coming from biotechnology renders their synthesis, analysis and modification straightforward. We thus engineered a series of bistable networks using the PEN DNA toolbox, a molecular programming language designed to construct networks analogous to transcriptional ones but using only simple biochemical reactions.[26] This technology has recently been applied to construct out-of-equilibirum networks displaying oscillations,[26,27] bistability[28] and traveling concentration waves.[17,25,29] Fig. 1b depicts the simplest bistable network used here, with a first-order positive feedback loop and a non-linear

repressor[30] (Supplementary Figs. 3-4). The nodes of the network, A_1 and R_1, are respectively 11 and 15-mer single-stranded DNAs (ssDNAs). Self-activation is set by T_{A_1}, a 22-mer ssDNA template. Repression is encoded by promoting the degradation of A_1 with a threshold given by R_1[30] —italized species names indicate concentration throughout the text. Three enzymes —a polymerase, an exonuclease and a nicking enzyme— catalyze the three basic reactions —DNA polymerization, ssDNA degradation and the nicking of double stranded DNA (dsDNA) in the presence of the correct recognition sequence— and dissipate free energy from a reservoir of deoxynucleoside triphosphates (dNTPs). In comparison with gene regulatory networks, template T_{A_1} plays the role of a gene, encoding information, A_1 and R_1 are analogous to transcription factors, as they promote or repress the activity of the template, and the three enzymes provide the metabolic functions homologous to the transcription-translation machinery. Moreover, A_1 is continuously produced and degraded but the total template —gene— concentration is fixed. In contrast to networks in vivo, molecular interactions are well-known and the mechanism and kinetic rates can be precisely determined.[26]

Our first goal was to create an immobile concentration front in the presence of a morphogen gradient, which we have called a Polish flag pattern. We performed patterning experiments within 5 cm-long sealed glass microchannels of 4×0.2 mm^2 cross-section (Fig. 1c). A gradient of morphogen R_1 was generated along the longitudinal axis of the channel, noted x, by partially mixing two solutions with different R_1 by Taylor dispersion (Fig. 1e and Supplementary Fig. 5). The gradient was well approximated by an exponential decay $e^{(x-x_0)/l}$ with characteristic length $l = 2$ cm. Because diffusion is slow over long distances the gradient was stable over 50 h (within 10% at the center of the channel, as expected for the diffusion of a 17-mer ssDNA, see Supplementary Fig. 5). Initially, the channel contained homogeneous concentrations of the three enzymes, dNTPs, $T_{A_1} = 25$ nM, $A_1 = 1$ nM, and a gradient of R_1 in the range $0-200$ nM. Throughout this work, the concentration of the network nodes, here A_1, was related to fluorescence intensity using two methods (see Methods). Either by adding the DNA intercalator EvaGreen, for which the fluorescence signal is proportional to the concentration of dsDNA, or by labeling one template with a fluorophore that is quenched upon hybridization. In order to facilitate the interpretation of the data we represent in all figures the fluorescence shift, which is the absolute value of the difference between the fluorescence intensity at a given time and at initial time.

As a consequence, at low concentration, the fluorescence shift is proportional to the concentration of the node species (see Methods). The fluorescence inside the channel was measured by recording time-lapse images with an inverted microscope. Fig. 1d displays the spatio-temporal dynamics of the patterning process. A short, purely reactional initial phase generated a sharp profile of A_1 at a location corresponding to low morphogen concentration (Supplementary Fig. 6). This profile later moved to the right through a RD mechanism, progressively decelerating until it stopped at the center of the channel at a position where $R_1^{RD} = 30 \pm 5$ nM. The front remained immobile up to 15 h and its characteristic width, defined as the decay length of a sigmoidal fit to the data, was $\lambda = 2$ mm, 10-fold sharper than the morphogen gradient (Fig. 1d and Supplementary Fig. 6). When, instead of the repressor, the autocatalyst template was used as the morphogen, the complementary Polish flag pattern was obtained (Supplementary Figs. 8-9).

The gap gene network, which interprets the Bicoid morphogen gradient during the development of the *Drosophila* blastoderm, is not composed of a unique self-activating and repressed node but of a series of them[31] (Supplementary Fig. 10). To demonstrate that our approach is capable of emulating the most basic type of such networks, we used one with two self-activating nodes, H and K, that repress each other[28] (Fig. 2a and Supplementary Fig. 11) and recorded the patterning dynamics in a gradient of the Bicoid analogue, T_H (Fig. 2b-d, Movie S1), the template corresponding to autocatalyst H. At short times, a purely reactional phase created two independent and sharp fronts of H and K. Subsequently, during an RD phase, the fronts traveled in opposite directions until they collided in the middle of the channel. At this time, the two profiles partially overlapped and a slow phase made the two fronts go backwards, repelling each other, until reaching a steady-state where the overlap disappeared. 1-dimensional simulations with a 4-variable model (Supplementary Section 3.1 and Supplementary Fig. 12) displayed a similar behavior and suggested that this last phase was due to a slow synthesis of the repressors (Fig. 2e-g). This patterning process was highly reproducible (Supplementary Figs. 13-14) and compatible with the immobilization of the morphogen gradient onto a surface (Supplementary Fig. 15).

To implement a French flag pattern with three chemically-distinct zones (Fig. 3) we combined two orthogonal bistables, A_2 and A_3, (Supplementary Fig. 16) into a single network using two different

approaches. We used a bifunctional morphogen bearing either both repressors, $\mathrm{R}_2 - \mathrm{R}_3$, or one autocatalyst template and a repressor, $\mathrm{T}_{A_2} - \mathrm{R}_3$. In a gradient of $\mathrm{R}_2 - \mathrm{R}_3$, a channel containing a uniform concentration of T_{A_2} and T_{A_3} generated a French flag pattern that divided space into three regions with different composition, $\mathrm{A}_2 + \mathrm{A}_3$, A_2 and $\emptyset$, for 100 min (Fig. 3a, Supplementary Figs. 17-18 and Supplementary Movie 2). By contrast, with a gradient of $\mathrm{T}_{A_2} - \mathrm{R}_3$ and a uniform concentration of R_2 and T_{A_3} a different pattern separated the space into A_3, $\mathrm{A}_2 + \mathrm{A}_3$ and A_2 (Fig. 3b).

In embryogenesis, pattern formation can induce tissue differentiation by providing localized chemical cues to pluripotent cells.[1] This strategy could be used for the autonomous fabrication of artificial materials. As a proof of concept we coupled the patterns obtained above to the conditional aggregation of 1 μm diameter beads[32] (Fig. 4). Streptavidin-labeled beads were decorated with two types of biotin-labeled DNAs that had two different 12-mer ssDNA dangling ends, B_i^l and B_i^r; for the pair of beads i, one has a *left* and the other a *right* strand. In the working buffer, the beads aggregated only in the presence of a linker strand L_i complementary to both *left* and *right* ssDNA portions (Supplementary Fig. 19). A capillary containing i) a homogeneous dispersion of beads B_i^l and B_i^r, ii) a bistable network with node A_j coupled to the linear production of L_i and iii) a gradient of R_j, produced a Polish flag of bead aggregation (Fig. 4c-e for $(i = 1, j = 1)$ and Supplementary Fig. 20 for $(i = 2, j = 3)$).

It is straightforward to generate two pairs of beads, (B_1^l, B_1^r) and (B_2^l, B_2^r), each pair aggregating independently of the other in the presence of its own linker (L_1 or L_2, Supplementary Fig. 21-23). The French flag pattern in Fig. 3a was thus materialized into three zones of space with distinct degree of aggregation (Fig. 4f and Supplementary Fig. 24): both pairs of beads aggregated / one pair of beads aggregated / no bead aggregated. In addition, bead aggregation brought two interesting properties. It allowed the visualization of RD patterns by eye (Supplementary Figs. 20 and 26) without the need of a fluorescence microscope and it froze the patterns into a state that was stable for at least one month, because aggregates precipitated to the bottom of the capillary (Supplementary Fig. 26). In other words: a steady-state dissipative structure of DNA was converted into a kinetically-trapped stable structure of beads.

Discussion

The object of synthesis in far from equilibrium chemistry is not anymore a molecular structure with desirable physico-chemical properties but a network of chemical reactions with particular dynamics. When these networks are coupled with some kind of transport —diffusion is just one possibility[33]— a length scale naturally emerges, which allows to structure space chemically. The first implication of our work is to provide an experimental framework for the synthesis of far from equilibrium chemical structures. Indeed, among the limited amount of frameworks that have been proposed to synthesize RD patterns,[34,35] few of them are both biocompatible and programmable. By programmable we mean that one may rationally choose which reactants will react with what mechanism to create a desired pattern. The PEN DNA toolbox used here is naturally biocompatible and DNA sequence complementarity makes it programmable —both for the topology of the network,[17,26,28] as shown in Fig. 1-4 and Supplementary Fig. 2, and for the reaction and diffusion rates.[25] Biocompatibility opens the way for the structuration of biomolecules and living cells with RD patterns. Programmability makes it suitable to synthesize new patterns, such as two-dimensional RD solitons,[36,37] to probe experimentally the degree of complexity that may emerge from RD patterning. The versatility of this method allows conceiving a new way of processing materials inspired from embryo development: embed them with an autonomous developmental program and let them construct themselves.

We may indeed consider embryogenesis as an extremely precise and autonomous procedure to structure matter. In contrast with current fabrication methods, it is able to position chemicals with multiscale precision —from tens of nm for cellular organelles to 10 μm for cells—, outstanding reproducibility and controlled dynamics without mechanical parts. In this regard, RD mechanisms have already been used to process materials, notably for micro- and nanofabrication using precipitation reactions.[38,39] Our approach significantly enlarges the complexity of the underlying reaction networks and, because information is encoded in DNA sequence, it could be coupled with directed evolution. If an autonomous fabrication method of this sort is once to find a real application it will need to build materials that are chemically diverse with a resolution at least comparable with the one in *Drosophila* patterning, which is 10 μm. Recent work demonstrates that it is possible to couple DNA species with

interesting chemistry such as DNA nanostructures,[40] aptamers,[41] hydrogels,[42] chemical synthesis[43] or gene delivery.[44] Although the current 2 mm resolution of our patterning chemistry is low, it is far from its theoretical limit. Indeed, RD patterning has been used for fabricating 300 nm objects.[38] The spatial resolution is determined by $\lambda \sim \sqrt{D/k}$, where k is the degradation rate (Supplementary Fig. 27). Here $\lambda = 2$ mm and taking $D = 1.8 \times 10^4$ μm^2/min for a 12-mer ssDNA[25] at 45°C one finds $k \approx 5 \times 10^{-3}$ min^{-1}. This value is in good agreement with the measured degradation kinetics of species W_2 in the presence of R_2, with rates in the $3 \times 10^{-2} - 3 \times 10^{-3}$ min^{-1} range (Supplementary Fig. 28). Improving the resolution down to 10 μm thus requires decreasing D and increasing k each by a factor 100, which is not unreasonable (Supplementary Fig. 28). In addition, coupling RD with other sharpening mechanisms could increase resolution further: the bead aggregation front was 4-fold sharper than the RD front, which may be due to the cooperativity of bead aggregation.[45] This multi-level sharpening recalls hierarchical patterning mechanisms in vivo. Incidentally, it appears plausible to make 100 μm-scale gradients by either using surface microprinting (Supplementary Fig. 15) or a self-generating diffusion-degradation mechanism.[46,47]

The second implication of our work is that it may help understanding the physics of chemical patterning in living systems.[48,49] Although our experimental system is an extreme simplification —no cells, no molecular crowding, no forces—, it integrates non-trivial microscopic interactions that are present in vivo —intra and inter-molecular forces, DNA hybridization and protein-DNA recognition— and all the time and spatial scales of reaction and diffusion are naturally included with actual molecules. It could thus provide an interesting framework to perform experimental simulations instead of computer ones when these have limitations, for instance when noise becomes important.

Conclusion

Our results demonstrate that DNA-based molecular programming is well-suited to engineer concentration patterns that emulate those observed during early embryo development. They indicate that the combination of a bistable reaction network with diffusion provides a simple engineer's solution to generate immobile concentration fronts that are both sharp and long lasting. Importantly, the simplic-

ity of the method allowed us to record the patterning dynamics in real time, showing that a purely reactional initial phase is followed by a reaction-diffusion one. Our experimental model may help understanding the role of regulative and diffusive processes during development and suggests that relatively simple networks may have enabled patterning at an early stage of evolution. Finally, by coupling programmable patterns with matter we have demonstrated a primitive autonomous chemical structuration of a material in one dimension. This approach could be exploited to fabricate soft materials following an autonomous developmental program.

Methods

DNA strands were purchased from Biomers (Ulm, Germany). The Bst DNA polymerase large fragment and the two nicking enzymes (Nb.BsmI and Nt.BstNBI) were purchased from New England Biolabs. The recombinant *Thermus thermophilus* RecJ exonuclease was produced as described.[50] Experiments were performed at 45 °C for the Polish and French flag generating networks and at 42 °C for those in Fig. 2. Details on the the sample preparation, the DNA sequences, the experimental conditions, the data analysis and the simulations are provided in the Supplementary Information.

Bead suspension. 1 μm diameter, streptavidin-coated, paramagnetic beads (Dynabeads MyOne C1, Invitrogen) were functionalized with two types of biotinylated DNA constructs, as described,[51] making a pair of beads, (B_i^l, B_i^r). Each construct consisted of a 49 bp-long dsDNA backbone terminated with a 12 bases-long single stranded sticky end. The construct corresponding to B_i^l (resp. B_i^r) was biotin-labeled on the 5' end (resp. 3' end) and the corresponding sticky end was on the 3' side (resp. 5' side).

Measurement of DNA concentrations. DNA concentrations were measured by fluorescence. To measure the concentration of autocatalytic nodes A_i, H and K we used two different strategies. i) All experiments involving A_i contained EvaGreen (Biotium), an intercalating dye which fluorescence is proportional to the concentration of dsDNA. ii) Some template strands were labeled with fluorescent dyes on their 3' or 5' ends (see Supplementary Table 2 for details) which fluorescence was quenched

specifically by the corresponding complementary strands. For experiments with networks involving a single node (Fig. 1) we used EvaGreen. For networks involving two nodes we either used two orthogonal N-quenching dyes (Fig. 2) or EvaGreen and an orthogonal N-quenching dye (Fig. 3). The concentration of morphogen was measured either by using a fluorescently-labeled strand (Fig. 2) or by adding a cascade blue-dextran $M_w = 3000$ Da (Thermo Fisher Scientific) (Fig. 1 and 3-4), and recording its fluorescence in real time. This fluorescent dextran has a diffusion coefficient similar to the DNA templates (Supplementary Fig. 5). All kymographs and plots display the fluorescence shift, i.e the absolute value of the difference between the fluorescence intensity at a given time and at initial time. The fluorescence shift is proportional to the concentration of the species of interest if this remains below the concentration of its complementary strand.

Generation of the morphogen gradient. Spatiotemporal experiments were performed within 50 mm $\times$ 4 mm $\times$ 0.2 mm glass capillaries (Vitrocom USA). One half of the capillary was loaded with the reaction solution without the morphogen strand and the other half with the same solution supplemented with the morphogen at 200 nM. To create the gradient the two solutions were mixed by applying a hydrodynamic flow along the capillary axis using a micropipette and a custom-made PDMS connector. 15 up-and-down pumps of 12.5 μL yielded a shallow morphogen gradient along the entire capillary length spanning between 0 and $\sim$100 nM. Subsequently, the capillaries were sealed with 5-minutes Araldite epoxy and glued over a 5×7.5 cm glass slide.

Microscopy. The fluorescence along the capillary was recorded on a Zeiss Axio Observer Z1 automated epifluorescence microscope equipped with a Tokai Hit thermo plate, an Andor iXon Ultra 897 EMCCD camera and a $2.5\times$ objective and controlled with MicroManager 1.4. For each capillary, 16 contiguous 3.17$\times$3.17 mm^2 images were recorded automatically every 1 to 10 minutes. Multi-color fluorescence microscopy was used to record the concentration of different DNA species over time. Images of the beads were acquired in bright field with a 10 or a $40\times$ objective.

Data treatment. The raw data were treated with ImageJ / Fiji (NIH) and Matlab (The Mathworks). The 16 images making one capillary were stitched together and corrected from inhomogeneous illumination. To obtain the kymographs, the images were averaged along the width of the capillary (y axis) and the corresponding profiles stacked over time. These profiles were further smoothed by performing a moving average along x, normalized and fitted to a sigmoid function $f(x) = \frac{1}{1+e^{(x-x_0)/\lambda}}$. The front position corresponds to x_0 and its width to λ. To determine the front velocity, the data of front position over time were fitted by a polynomial function to reduce noise. The velocity was calculated as the time derivative of this polynomial fit. To plot the bead aggregation profile along the capillary, the corresponding brightfield images were first binarized and the number of particles counted in areas 100 μm wide. A particle here indicates either an aggregate or a bead: the number of aggregates was thus inversely proportional to the number of detected particles.

Data availability. All data generated or analysed during this study are included in this published article (and its supplementary information files). The raw datasets and the plasmid for expressing ttRecJ are available from the corresponding authors on reasonable request.

Acknowledgments

We thank E. Frey for insightful discussions, A. Vlandas for help with gradient generation and B. Caller and D. Woods for comments on the text. Supported by European commission FET-STREP (Ribonets), by ANR jeunes chercheurs program (Dynano), by C'nano Ile-de-France (DNA2PROT) and by Ville de Paris Emergences program (Morphoart). Correspondence and requests should be addressed to A.E.-T. (andre.estevez-torres@upmc.fr) or J.-C.G (jean-christophe.galas@upmc.fr).

Author contributions

A.S.Z., J.-C.G. and A.E.-T. performed most experiments and analyzed the data. Y.R. and G.G. designed the network in Fig. 1 and J.-C.G. and A.E.-T. designed the networks in Figs. 3-4. A.Z. and V.D. set up the bead experiments. G.U. performed critical control experiments. All the authors discussed

the results. J.-C.G., A.S.Z., Y.R. and A.E.-T. designed research and J.-C.G. and A.E.-T. wrote the manuscript.

Competing financial interests

The authors declare no competing financial interests.

Table of contents summary

During embryogenesis patterns of protein concentration appear in response to morphogen gradients, providing spatial and chemical information that directs the fate of the underlying cells. Here, this process is emulated with DNA-based non-living matter and the autonomous structuration of a synthetic material is demonstrated.

References

[1] Wolpert, L. & Tickle, C. *Principles of development* (Oxford University Press, Oxford, 2011).

[2] Tompkins, N. *et al.* Testing Turing's theory of morphogenesis in chemical cells. *Proc. Natl. Acad. Sci. U. S. A.* **10.1073/pnas.1322005111** (2014).

[3] Yoshida, R., Takahashi, T., Yamaguchi, T. & Ichijo, H. Self-oscillating gel. *J. Am. Chem. Soc.* **118**, 5134–5135 (1996).

[4] Inostroza-Brito, K. E. *et al.* Co-assembly, spatiotemporal control and morphogenesis of a hybrid protein-peptide system. *Nat Chem* **7**, 897–904 (2015).

[5] Turing, A. M. The chemical basis of morphogenesis. *Phil. Trans. Roy. Soc. B* **237**, 37–72 (1952).

[6] Wolpert, L. Positional information and the spatial pattern of cellular differentiation. *J. Theo. Biol.* **25**, 1–47 (1969).

[7] Green, J. B. & Sharpe, J. Positional information and reaction-diffusion: two big ideas in developmental biology combine. *Development* **142**, 1203–11 (2015).

[8] Rulands, S., Klünder, B. & Frey, E. Stability of localized wave fronts in bistable systems. *Phys. Rev. Lett.* **110**, 038102 (2013).

[9] Quiñinao, C., Prochiantz, A. & Touboul, J. Local homeoprotein diffusion can stabilize boundaries generated by graded positional cues. *Development* **142**, 1860–8 (2015).

[10] Sheth, R. *et al.* Hox genes regulate digit patterning by controlling the wavelength of a Turing-type mechanism. *Science* **338**, 1476–1480 (2012).

[11] Economou, A. D. *et al.* Periodic stripe formation by a Turing mechanism operating at growth zones in the mammalian palate. *Nat. Genet.* **44**, 348–351 (2012).

[12] Johnston, D. S. & Nüsslein-Volhard, C. The origin of pattern and polarity in the drosophila embryo. *Cell* **68**, 201–219 (1992).

[13] Briscoe, J. & Small, S. Morphogen rules: design principles of gradient-mediated embryo patterning. *Development* **142**, 3996–4009 (2015).

[14] Castets, V., Dulos, E., Boissonade, J. & De Kepper, P. Experimental evidence of a sustained standing Turing-type nonequilibrium chemical pattern. *Phys. Rev. Lett.* **64**, 2953 (1990).

[15] Isalan, M., Lemerle, C. & Serrano, L. Engineering gene networks to emulate drosophila embryonic pattern formation. *PLoS Biol.* **3**, 488–496 (2005).

[16] Loose, M., Fischer-Friedrich, E., Ries, J., Kruse, K. & Schwille, P. Spatial regulators for bacterial cell division self-organize into surface waves in vitro. *Science* **320**, 789–792 (2008).

[17] Padirac, A., Fujii, T., Estevez-Torres, A. & Rondelez, Y. Spatial waves in synthetic biochemical networks. *J. Am. Chem. Soc.* **135**, 14586–14592 (2013).

[18] Chirieleison, S. M., Allen, P. B., Simpson, Z. B., Ellington, A. D. & C., X. Pattern transformation with DNA circuits. *Nat Chem* **5**, 1000–1005 (2013).

[19] Semenov, S. N., Markvoort, A. J., de Greef, T. F. A. & Huck, W. T. S. Threshold sensing through a synthetic enzymatic reaction-diffusion network. *Angew. Chem. Intl. Ed.* **53**, 8066–8069 (2014).

[20] Tayar, A. M., Karzbrun, E., Noireaux, V. & Bar-Ziv, R. H. Propagating gene expression fronts in a one-dimensional coupled system of artificial cells. *Nat. Phys.* **11**, 1037–1041 (2015).

[21] Lewis, J., Slack, J. M. W. & Wolpert, L. Thresholds in development. *J. Theor. Biol.* **65**, 579–590 (1977).

[22] François, P., Hakim, V. & Siggia, E. D. Deriving structure from evolution: metazoan segmentation. *Mol. Syst. Biol.* **3**, 154 (2007).

[23] Lopes, F. J., Vieira, F. M., Holloway, D. M., Bisch, P. M. & Spirov, A. V. Spatial bistability generates hunchback expression sharpness in the drosophila embryo. *PLoS Comput. Biol.* **4**, e1000184 (2008).

[24] Scalise, D. & Schulman, R. Designing modular reaction-diffusion programs for complex pattern formation. *Technology* **02**, 55–66 (2014).

[25] Zadorin, A. S., Rondelez, Y., Galas, J.-C. & Estevez-Torres, A. Synthesis of programmable reaction-diffusion fronts using DNA catalyzers. *Phys. Rev. Lett.* **114**, 068301 (2015).

[26] Montagne, K., Plasson, R., Sakai, Y., Fujii, T. & Rondelez, Y. Programming an in vitro DNA oscillator using a molecular networking strategy. *Mol. Syst. Biol.* **7**, 466 (2011).

[27] Fujii, T. & Rondelez, Y. Predator-prey molecular ecosystems. *ACS Nano* **7**, 27–34 (2013).

[28] Padirac, A., Fujii, T. & Rondelez, Y. Bottom-up construction of in vitro switchable memories. *Proc. Natl. Acad. Sci. USA* **10.1073/pnas.1212069109** (2012).

[29] Zambrano, A., Zadorin, A. S., Rondelez, Y., Estevez-Torres, A. & Galas, J. C. Pursuit-and-evasion reaction-diffusion waves in microreactors with tailored geometry. *J. Phys. Chem. B* **119**, 5349–5355 (2015).

[30] Montagne, K., Gines, G., Fujii, T. & Rondelez, Y. Boosting functionality of synthetic DNA circuits with tailored deactivation. *Nat. Comm.* **7**, 13474 (2016).

[31] Manu *et al.* Canalization of gene expression and domain shifts in the drosophila blastoderm by dynamical attractors. *PLoS Comput. Biol.* **5**, e1000303 (2009).

[32] Mirkin, C. A., Letsinger, R. L., Mucic, R. C. & Storhoff, J. J. A DNA-based method for rationally assembling nanoparticles into macroscopic materials. *Nature* **382**, 607–609 (1996).

[33] Howard, J., Grill, S. W. & Bois, J. S. Turing's next steps: the mechanochemical basis of morphogenesis. *Nat. Rev. Mol. Cell Biol.* **12**, 392–398 (2011).

[34] Vanag, V. K. & Epstein, I. R. Pattern formation mechanisms in reaction-diffusion systems. *Int. J. Dev. Biol.* **53**, 673–681 (2009).

[35] van Roekel, H. W. H. *et al.* Programmable chemical reaction networks: emulating regulatory functions in living cells using a bottom-up approach. *Chem. Soc. Rev.* **44**, 7465–7483 (2015).

[36] Rotermund, H. H., Jakubith, S., von Oertzen, A. & Ertl, G. Solitons in a surface reaction. *Phys. Rev. Lett.* **66**, 3083–3086 (1991).

[37] Descalzi, O., Akhmediev, N. & Brand, H. R. Exploding dissipative solitons in reaction-diffusion systems. *Phys. Rev. E* **88**, 042911 (2013).

[38] Grzybowski, B. A., Bishop, K. J. M., Campbell, C. J., Fialkowski, M. & Smoukov, S. K. Micro- and nanotechnology via reaction-diffusion. *Soft Matter* **1**, 114–128 (2005).

[39] Nakouzi, E. & Steinbock, O. Self-organization in precipitation reactions far from the equilibrium. *Science Advances* **2** (2016).

[40] Rothemund, P. W. K. Folding DNA to create nanoscale shapes and patterns. *Nature* **440**, 297–302 (2006).

[41] Franco, E. *et al.* Timing molecular motion and production with a synthetic transcriptional clock. *Proc. Natl. Acad. Sci. USA* **10.1073/pnas.1100060108** (2011).

[42] Lee, J. B. *et al.* A mechanical metamaterial made from a DNA hydrogel. *Nat. Nanotech.* **7**, 816–820 (2012).

[43] Gartner, Z. J. & Liu, D. R. The generality of DNA-templated synthesis as a basis for evolving non-natural small molecules. *J. Am. Chem. Soc.* **123**, 6961–6963 (2001).

[44] Patwa, A., Gissot, A., Bestel, I. & Barthelemy, P. Hybrid lipid oligonucleotide conjugates: synthesis, self-assemblies and biomedical applications. *Chem. Soc. Rev.* **40**, 5844–5854 (2011).

[45] Jin, R., Wu, G., Li, Z., Mirkin, C. A. & Schatz, G. C. What controls the melting properties of DNA-linked gold nanoparticle assemblies? *J. Am. Chem. Soc.* **125**, 1643–1654 (2003).

[46] Wartlick, O., Kicheva, A. & González-Gaitán, M. Morphogen gradient formation. *Cold Spring Harbor Perspectives in Biology* **1** (2009).

[47] Gines, G. *et al.* Microscopic agents programmed by DNA circuits. *Nat Nano* **advance online publication** (2017).

[48] Giurumescu, C. A. & Asthagiri, A. R. *Chapter 14 - Systems Approaches to Developmental Patterning*, 329–350 (Academic Press, San Diego, 2010).

[49] Shvartsman, S. Y. & Baker, R. E. Mathematical models of morphogen gradients and their effects on gene expression. *Wiley Interdisciplinary Reviews: Developmental Biology* **1**, 715–730 (2012).

[50] Wakamatsu, T. *et al.* Structure of RecJ exonuclease defines its specificity for single-stranded DNA. *J. Biol. Chem.* **285**, 9762–9 (2010).

[51] Leunissen, M. E. *et al.* Towards self-replicating materials of DNA-functionalized colloids. *Soft Matter* **5**, 2422 (2009).

Figure captions

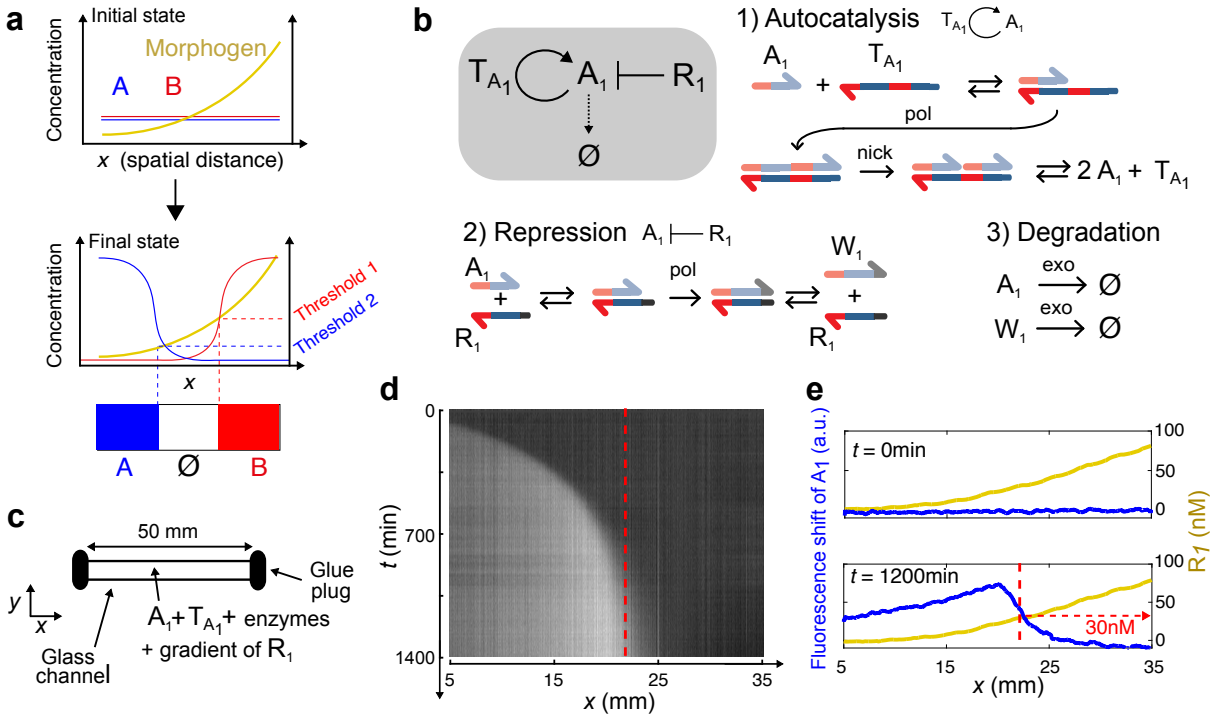

Figure 1: In a shallow gradient of morphogen, a bistable DNA network produces a Polish flag; a sharp and immobile concentration profile. **a**, Scheme of Wolpert's French flag problem, where a gradient of morphogen yields three chemically-distinct zones: blue, white and red. **b**, Molecular mechanism of a DNA-based bistable network where A_1 self-activation is supported by template T_{A_1} and A_1 is repressed by R_1 and continuously degraded. Harpooned thick arrows are ssDNA where colors indicate sequence domains and light hue indicates complementarity. Straight black arrows denote chemical reactions. pol, nick and exo stand for polymerase, nicking enzyme and exonuclease, respectively. W_1 is a waste strand that cannot activate T_{A_1}. **c**, Sketch of the experimental setup. **d**, Kymograph of the fluorescence shift due to A_1 inside a capillary containing the network in **b** with homogeneous initial condition $A_1(x, t = 0) = 1$ nM and pre-patterned with the gradient $R_1(x, t = 0)$ as in **e**. The red dashed line indicates the stationary position of the profile. **e**, Profiles of R_1 (yellow) and the fluorescence shift due to A_1 (blue) along the channel at initial time and after 1200 min.

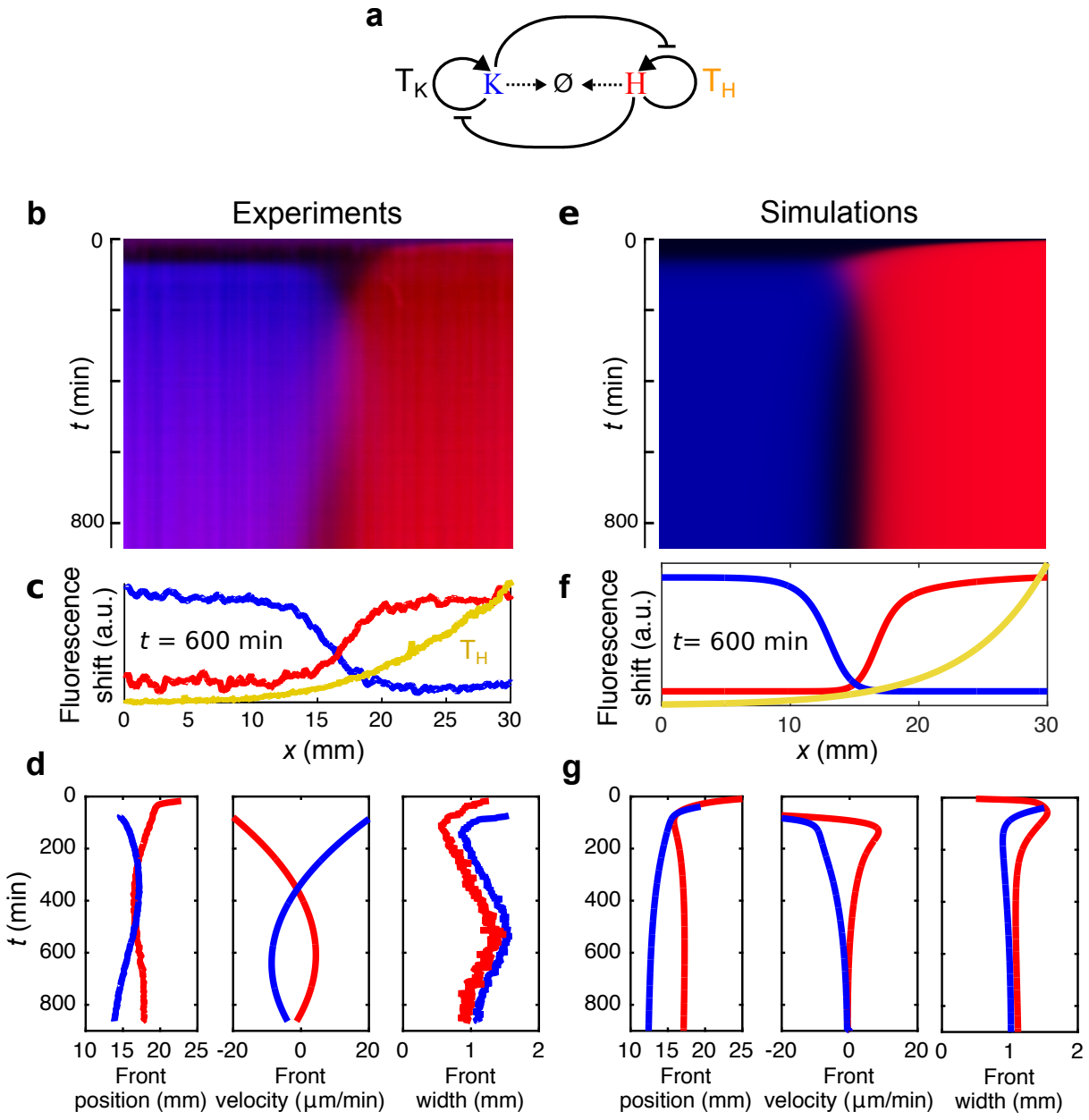

Figure 2: A DNA-based network with two self-activating nodes that repress each other generates two immobile fronts that repel each other. **a**, Reaction network used here where H and K self-activate on their templates T_H and T_K and repress each other. Experiments (**b**, **c**, **d**) and simulations (**e**, **f**, **g**) showing the kymograph of the fluorescence shift (**b**, **e**) for species H (red) and K (blue) inside a capillary containing the network in **a** and pre-patterned with a gradient of T_H (yellow) and the fluorescence shift profiles at $t = 600$ min (**c**, **f**). **d**, **g**, Front position, velocity and width as a function of time extracted from the kymograph (colors as in **c** and **f**).

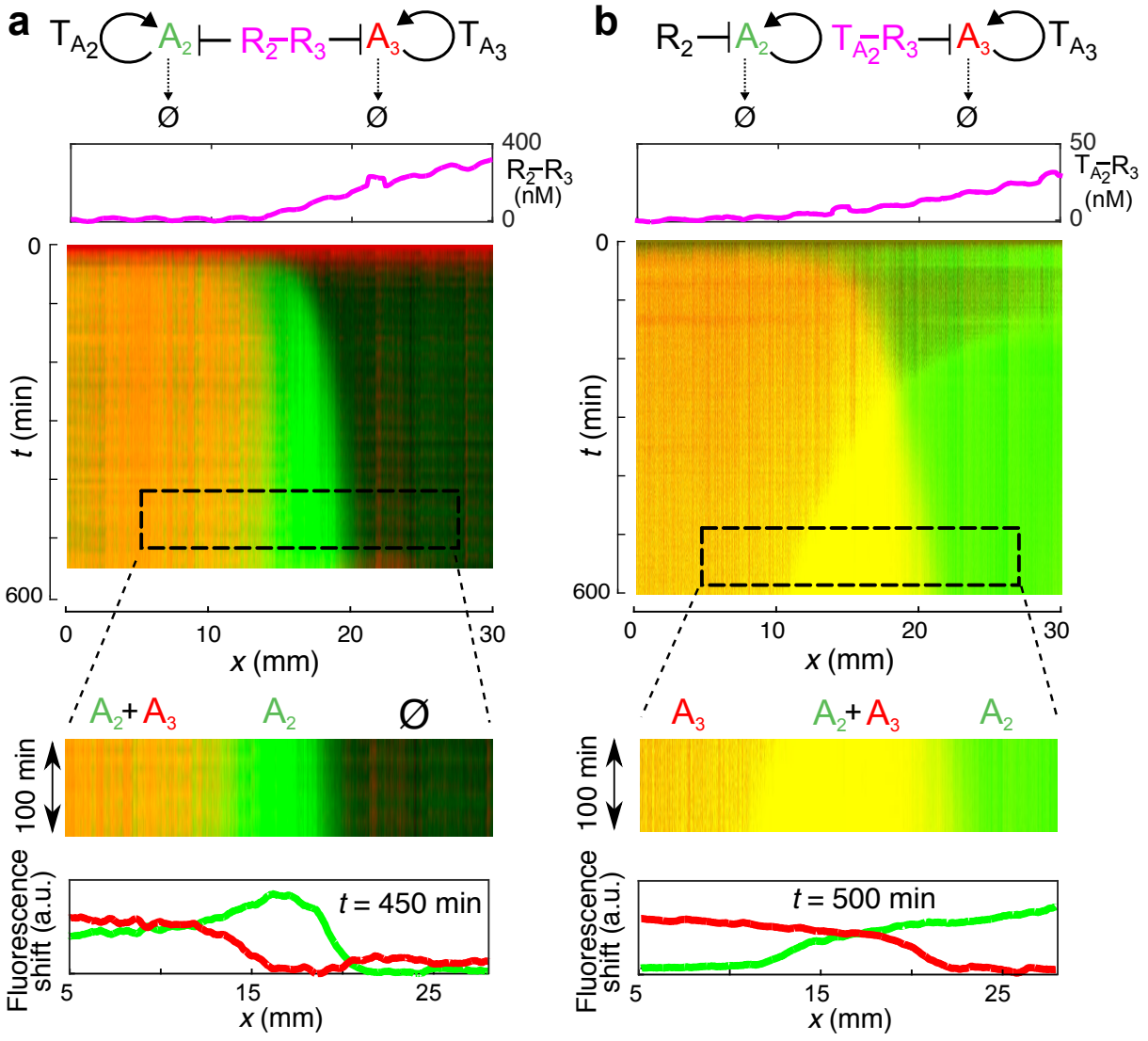

Figure 3: The combination of two orthogonal bistable networks produces a French flag pattern of DNA concentration that can be simply reprogrammed. From top to bottom: network topology, initial morphogen gradient, kymograph and fluorescence shift profiles at steady state for two bistables coupled through either a double-repressor strand, $\mathrm{R}_2 - \mathrm{R}_3$, **a**, or a template-repressor strand, $\mathrm{T}_{A_2} - \mathrm{R}_3$, **b**, each used as morphogen in the gradient. Dashed rectangles are zooms of the kymographs where the two French flag patterns were stationary.

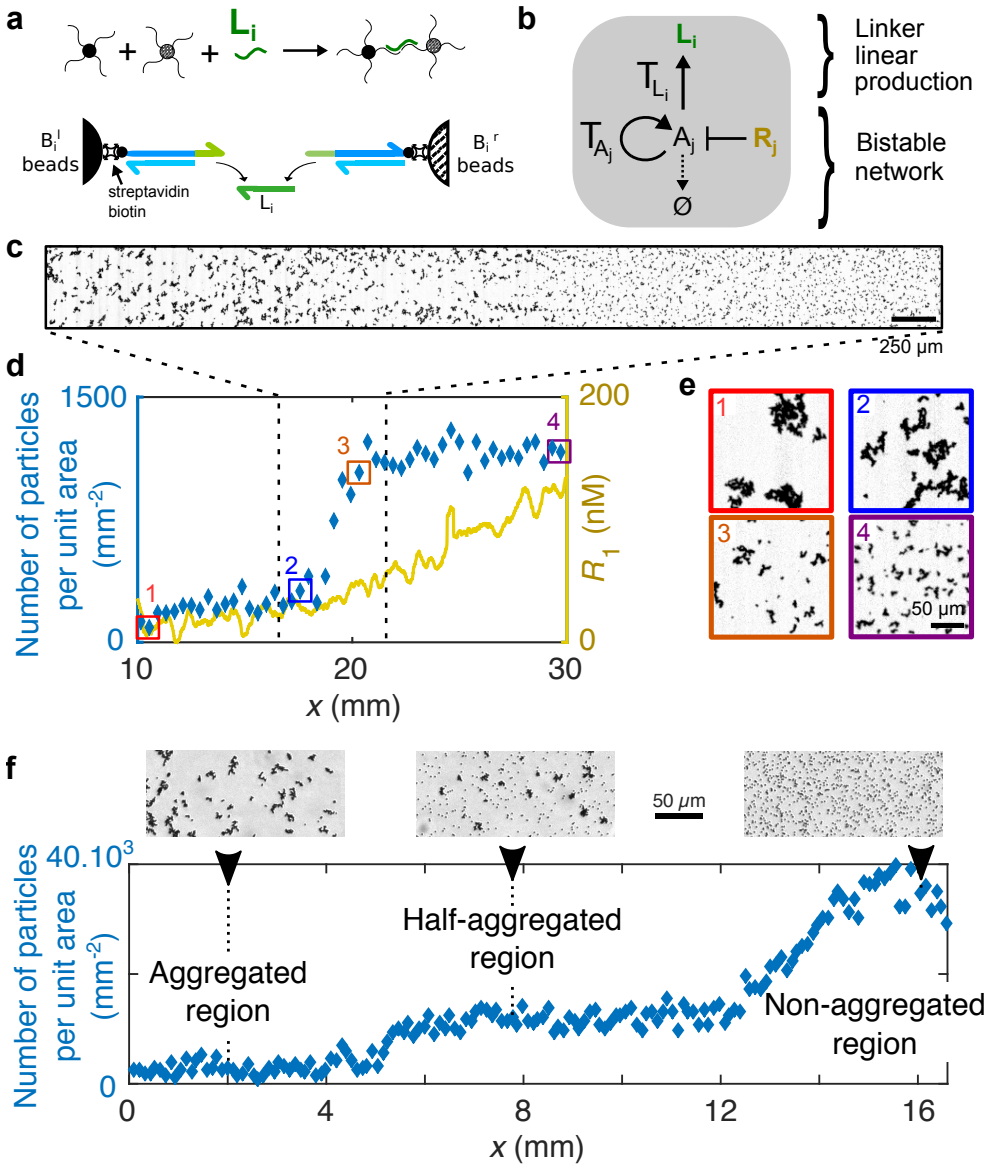

Figure 4: Materialization of a Polish and a French flag pattern with conditional bead aggregation. **a**, Sketch of the mechanism of bead aggregation where a pair i of 1 μm beads decorated with two different DNA constructs (black and gray disks) are aggregated in the presence of linker strand L_i. **b**, Scheme of the reaction network motif used to couple a bistable network based on species A_j with the linear production of L_i supported by template $\mathrm{T}_{\mathrm{L}_i}$. **c-e**, Polish flag pattern of bead aggregation obtained after 40 h in a channel containing the beads $i = 1$ and a network $j = 1$ with an initial gradient of R_1. **c**, Brightfield image at the center of the channel. **d**, Number of particles per unit area (blue diamonds, left axis) and initial concentration of R_1 (yellow line, right axis) along the longitudinal axis of the channel. The colored squares indicate the positions at which the brighfield images in **e** were recorded. The dashed lines correspond to the position where **c** was recorded. **f**, French flag pattern of bead aggregation obtained after 40 h in a channel containing the beads $i = (1, 2)$ and two networks $j = (1, 3)$ with initial gradients of R_1 and R_3.